

# Low-temperature solid state synthesis and *in situ* phase transformation to prepare nearly pure cBN<sup>†</sup>

Gang Lian,<sup>a,b</sup> Xiao Zhang,<sup>b</sup> Miao Tan,<sup>a</sup> Shunjie Zhang,<sup>b</sup> Deliang Cui<sup>\*a</sup> and Qilong Wang<sup>\*b</sup>

Received 23rd December 2010, Accepted 19th April 2011

DOI: 10.1039/c0dt01823f

Cubic boron nitride (cBN) is synthesized by a low-temperature solid state synthesis and *in situ* phase transformation route with NH<sub>4</sub>BF<sub>4</sub>, B, NaBH<sub>4</sub> and KBH<sub>4</sub> as the boron sources and NaN<sub>3</sub> as the nitrogen source. Furthermore, two new strategies are developed, *i.e.*, applying pressure on the reactants during the reaction process and introducing the structural induction effect. These results reveal that the relative contents of cBN are greatly increased by applying these new strategies. Finally, almost pure cBN (~90%) crystals are obtained by reacting NH<sub>4</sub>BF<sub>4</sub> and NaN<sub>3</sub> at 250 °C and 450 MPa for 24 h, with NaF as the structural induction material. The heterogeneous nucleation mechanism can commendably illuminate the structure induction effect of NaF with face center cubic structure. In addition, the induction effect results in the cBN nanocrystals presenting obvious oriented growth of {111} planes.

## 1. Introduction

Boron nitride (BN) has many polymorphs, including sp<sup>2</sup>-bonded hexagonal BN (hBN), turbostratic BN (tBN) and sp<sup>3</sup>-bonded cubic BN (cBN) and wurtzite BN (wBN). Among them, cBN, structurally analogous to diamond, has strong covalent bonds which makes it an attractive material with excellent properties. Only next to diamond, cBN possesses the second best hardness, elastic modulus and thermal conductivity, but it is superior to diamond for its higher oxidation temperature and chemical inertness to molten ferrous metals. These merits make cBN the best material for fabricating cutting tools, protective coatings and heat-sinks of high power electronic devices *etc.* Besides, the wide bandgap (~6.2 eV), high carrier mobility, p- and n- conductivity modifications endow cBN with the functions of being fabricated into ultraviolet optoelectronic devices<sup>1–8</sup> *etc.*

Conventionally, cBN was prepared by directly converting hBN under high-temperature and high-pressure.<sup>9</sup> It is well known that hBN is a stable phase at ambient temperature and pressure, and a high energy barrier exists between hBN and cBN, thus rather harsh conditions are required for such a phase transformation (for example, 10 GPa & 3000 °C was required for the direct transformation). Although the temperature and pressure obviously decreased by utilizing some catalysts (Mg, Mg–Al, MgB<sub>2</sub>, Mg<sub>3</sub>N<sub>2</sub>, Li<sub>3</sub>N, AlN *etc.*),<sup>10–15</sup> replacing well crystallized hBN with low ordered tBN or aBN<sup>16–17</sup> and introducing supercritical fluids

(liquid ammonia, hydrazine *etc.*),<sup>18</sup> the conditions are still too harsh (>800 °C & >1000 MPa). Thereby, it will be of high practical value to develop a facile and effective route to fabricate cBN under moderate conditions.

According to the phase diagram of BN, hBN and tBN are stable phases at ambient pressure, and cBN is stable at high pressure. So, generally, it is believed that the conventional low-temperature solid state reaction route always results in the formation of hBN or tBN<sup>19–22</sup> (sp<sup>2</sup>-hybrid). However, we have successfully obtained cBN nanocrystals by a modified low-temperature solid state reaction route (namely the reactants pressed into dense pellets). Furthermore, we also discuss what would be the result if pressure was applied to the reactants during the synthesis of BN. Actually, Kaner *et al.*<sup>23–24</sup> have successfully synthesized some high-pressure phase nitrides with cubic structures (GaN, TaN, CrN, Mo<sub>2</sub>N) by adding pressure. In addition, the structural induction effect is successfully applied in promoting the deposition of the cBN film.<sup>25–28</sup> So, would this induction effect be useful to promote the formation of cBN in our solid state system? Based on these considerations, we developed a low-temperature solid state synthesis and *in situ* phase transformation route, by applying a constant pressure on the reactants and introducing the structural induction effect during the synthesis of BN. As a result, nearly pure cBN nanocrystals have been successfully prepared by a low-temperature solid state route for the first time.

## 2. Experimental section

### 2.1 Synthesis of BN at low temperature with the reactants pressed into dense pellets

All the chemicals were of analytical grade (A.R.) and without further purification prior to use, and the experimental parameters

<sup>a</sup>State Key Lab of Crystal Materials, Shandong University, Shanda Nanlu No.27, Jinan, 250100, P. R. China. E-mail: cuidl@sdu.edu.cn; Fax: (+86)531-88361856; Tel: (+86)531-88361856

<sup>b</sup>School of Chemistry and Chemical Engineering, Shandong University, Shanda Nanlu No.27, Jinan, 250100, P. R. China. E-mail: gang\_lian2000@yahoo.com.cn; Tel: (+86)531-88365899

<sup>†</sup> Electronic supplementary information (ESI) available. See DOI: 10.1039/c0dt01823f

**Table 1** Key parameters of the experiments

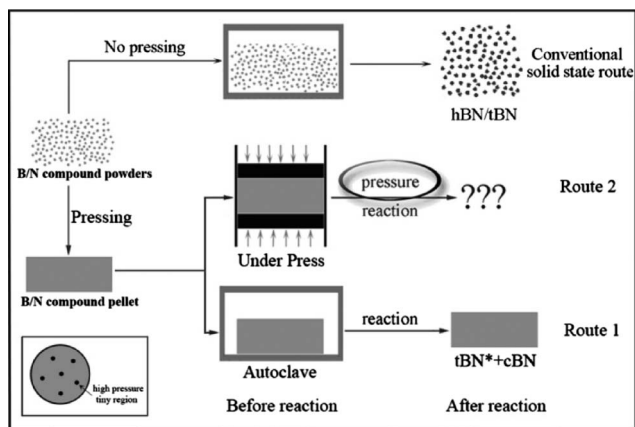
No.	Reactants	Pressed	$T$ (°C)	$t$ (h)	Phases <sup>a</sup>
S-1	1NH <sub>4</sub> BF <sub>4</sub> : 4NaN <sub>3</sub>	Y	250	24	tBN*+cBN
S-2	1NaBH <sub>4</sub> : 3NaN <sub>3</sub>	Y	250	24	tBN*+cBN
S-3	1KBH <sub>4</sub> : 3NaN <sub>3</sub>	Y	250	24	tBN*+cBN
S-4	1B: 3NaN <sub>3</sub>	Y	250	24	tBN*+cBN
S-5	1B: 3NaN <sub>3</sub>	Y	250	24 × 6	tBN+cBN*

<sup>a</sup> \* Denotes the dominant phase(s).

can be found in Table 1. In a typical synthesis, 5 mmol ammonium tetrafluoroborate (NH<sub>4</sub>BF<sub>4</sub>) and 20 mmol sodium azide (NaN<sub>3</sub>) were mixed together and pressed into dense pellets. Then the pellets were placed in an N<sub>2</sub>-flowing glove box (the concentration of both moisture and oxygen was less than 1 ppm) to eliminate the adsorbed water and oxygen, followed by sealing the pellets into a stainless steel reaction autoclave. Afterwards, the autoclave was heated at a rate of 3 °C min<sup>-1</sup> to 250 °C and held for 24 h, followed by cooling the autoclave to room temperature naturally. Finally, the product was washed successively with hydrochloric acid (HCl) and deionized water several times to remove the byproducts and impurities. After heating at 80 °C for 8 h, the BN sample was obtained. It was quite amazing that a small amount of the cubic phase of BN was detected in the sample prepared at a temperature as low as 250 °C, and the cubic phase of BN was also observed in the samples prepared by the same route, using NaBH<sub>4</sub>, KBH<sub>4</sub> and B as the boron sources (ESI S-1†).

## 2.2 Preparing the cubic phase of BN by applying pressure on the reactants and introducing the structural induction effect (*in situ* phase transformation)

In another typical synthesis, 5 mmol NH<sub>4</sub>BF<sub>4</sub> and 20 mmol NaN<sub>3</sub> were used as the reactants, and the experimental process was similar to that described above, except that a constant pressure was applied on the dense pellets during the reaction process (Route 2 in Scheme 1). Using this method, a series of BN samples were prepared by varying the temperature, pressure and reaction duration, and the detailed experimental parameters are shown in Table 2.



**Scheme 1** Schematic of the solid state reaction for synthesizing BN. Route 1: modified low-temperature solid state reaction route; Route 2: modified low-temperature solid state reaction route with assistance of pressure.

**Table 2** Key parameters of preparing BN samples

No.	NH <sub>4</sub> BF <sub>4</sub> /NaN <sub>3</sub>	$T$ (°C)	$t$ (h)	$P$ (MPa)	Phases <sup>a</sup>
S-6	1/4	220	24	0	t*BN+cBN
S-7	1/4	220	24	125	t*BN+cBN
S-8	1/4	220	24	300	t*BN+cBN
S-9	1/4	220	24	450	tBN+cBN
S-10	1/4	220	48	450	tBN+cBN*
S-11	1/4	250	24	0	t*BN+cBN
S-12	1/4	250	24	125	t*BN+cBN
S-13	1/4	250	24	300	t*BN+cBN
S-14	1/4	250	24	450	t*BN+cBN
S-15	1/4	250	48	450	tBN+cBN*
S-16	1/4	300	24	0	tBN
S-17	1/4	300	24	125	t*BN+cBN
S-18	1/4	300	24	300	t*BN+cBN
S-19	1/4	300	24	450	t*BN+cBN
S-20	1/4	300	48	450	tBN+cBN

<sup>a</sup> \* Denotes the dominant phase in the sample.

Furthermore, 5 mmol NaF, which was used as the structural induction material, was introduced into the reactants, and the synthesis was carried out at 250 °C under 125 MPa and 450 MPa, respectively.

## 2.3 Characterization of the samples

Phases of the sample were identified by X-ray powder diffraction (XRD) patterns, which were obtained on a Rigaku D/max-γA X-ray diffractometer with Ni filtered Cu-Kα radiation ( $V = 40$  kV,  $I = 50$  mA). Besides, infrared (IR) absorption spectra, collected on a Nicolet NEXUS 670 Fourier transformation infrared spectrometer, were also used to determine the structural information of samples. On the other hand, the X-ray photoelectron spectra (XPS), collected on a ThermoFisher ESCALAB 250 equipment, were employed to verify the elemental and phase composition of samples. The morphology of the samples was observed by a JSM-6700F field emission scanning electron microscope (SEM, ×200 k) and a Hitachi H-800 transmission electron microscope (TEM, 150 kV). Lattice fringes were observed by a Phillips Tecnai Twin-20U high resolution transmission electron microscope (HRTEM, 200 kV). Prior to the measurement of SEM, TEM and HRTEM, the samples were ultrasonically treated in ethanol for 30 min.

## 3. Results and discussion

### 3.1 Identification of the phase compositions

Via the modified low-temperature solid state reaction route, we have prepared BN using NH<sub>4</sub>BF<sub>4</sub> and NaN<sub>3</sub> as the reactants, the detailed parameters of the experiments are presented in Table 1 and the reaction can be expressed as follows:



Firstly, the XRD pattern has been employed to identify the phase compositions of the sample, and the typical XRD pattern of sample S-1 is shown in Fig. 1(a). Only two broad diffraction peaks at  $2\theta$  of 24–27° and 40–46° imply a typical tBN structure. Although the two peaks match well the (002) and (100) plane spacings of a crystalline hBN, the measured interlayer distance of  $d_{002}$  is ~3.51 Å and is obviously larger than ~3.33 Å, which is

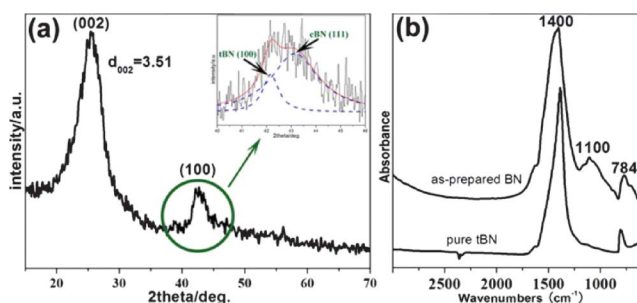


**Fig. 1** Phase composition of sample S-1. (a) XRD pattern. Inset shows that the peak of 40–46° can be fitted to the (100) plane of tBN and (111) plane of cBN; (b) FTIR spectra. Top: mixed phase (tBN+cBN) BN of sample S-1 prepared by modified solid state reaction route; bottom: pure phase tBN prepared by traditional solid state reaction route.

peculiar to well-crystalline hBN.<sup>30</sup> The BN phase formation can be further confirmed by the FTIR analyses, as depicted in Fig. 1(b). The dominant vibrations at  $\sim 1400\text{ cm}^{-1}$  and  $\sim 784\text{ cm}^{-1}$  are assigned to the  $\nu(\text{B-N})$  and  $\delta(\text{B-N})$  modes of tBN, which verifies that the major phase in the as-prepared sample S-1 is tBN. But, except for the characteristic B–N vibrations of tBN, it is worth noting that a weak peak centered at  $\sim 1100\text{ cm}^{-1}$  is observed, which can be attributed to the characteristic absorption of the transverse optical (TO) phonon of cBN.<sup>31–32</sup> It is quite exciting to obtain cBN at 250 °C.

In addition, XPS analysis is also used to determine the elemental compositions and chemical bondings of sample S-1. Fig. 2(a) shows the survey scan XPS spectrum. Besides the weak peaks of  $\text{O}_{1s}$  and  $\text{C}_{1s}$ , from the  $\text{CO}_2$  and  $\text{O}_2$  adsorbed on the surface of the sample, two dominant strong peaks of  $\text{B}_{1s}$  and  $\text{N}_{1s}$  indicate that the sample is composed of B and N elements. The binding energies of  $\text{B}_{1s}$  (190.3 eV) and  $\text{N}_{1s}$  (398.0 eV) are in good agreement with the values of bulk BN.<sup>29</sup> The quantification of peaks confirms that the atomic ratio of B : N is  $\sim 1.02 : 1$ , which is very close to the chemical stoichiometry of BN. Fig. 2(b–c) shows the 1s core spectra of B and N. The dissymmetric peaks suggest that there is more than one type of bonding scheme for the B and N atoms. The XPS spectra were therefore fitted to investigate possible chemical bonding and phase compositions of sample S-1. The fitting results of the  $\text{B}_{1s}$  and  $\text{N}_{1s}$  spectra give two group peaks centered at 190.2 eV & 191.5 eV (inset in Fig. 2(b)), and 397.9 eV & 398.8 eV (inset in Fig. 2(c)), respectively. According to the NIST database, the lower bonding energies of  $\text{B}_{1s}$  (190.2 eV) and  $\text{N}_{1s}$  (397.9 eV) can be attributed

to  $\text{sp}^2$ -bonded BN (low symmetric turbostratic phase) and the higher bonding energies of  $\text{B}_{1s}$  (191.5 eV) and  $\text{N}_{1s}$  (398.8 eV) are contributed by  $\text{sp}^3$ -bonded cBN (high symmetric cubic phase). So, the XPS results are in good agreement with the former FTIR analysis.

In order to examine the applicability of the modified solid state reaction route, we tried to synthesize cBN by using other boron sources such as  $\text{NaBH}_4$ ,  $\text{KBH}_4$  and B, and the reaction proceeded at 250 °C for 24 h with the reactants pressed into dense pellets. The results show that, besides the dominant phase of tBN in the as-prepared samples S-2, S-3 and S-4, the cubic phase is also detected (ESI S-1†). Comparatively, when the reaction duration is prolonged to 144 h, then cBN becomes the major phase in sample S-5 with B as the boron source. Unfortunately, the yield of BN sample (tBN+cBN) is very poor due to the low activity of B at 250 °C. In consideration of the yield and activity of reactants,  $\text{NH}_4\text{BF}_4$  is selected as the boron source in the following experiments.

Based on the above experimental results, we believe that an *in situ* phase transformation process achieves the formation of the cubic phase of BN. So, we schematically depict the solid state reaction process in Scheme 1. Because the reaction temperature (250 °C) is lower than the decomposition temperatures of  $\text{NH}_4\text{BF}_4$  ( $>307\text{ °C}$ ) and  $\text{NaN}_3$  ( $>283\text{ °C}$ ),<sup>33</sup> the exothermic reaction between  $\text{NH}_4\text{BF}_4$  and  $\text{NaN}_3$  might have proceeded slowly at 250 °C. Thus the pellet configuration is preserved after reaction (Route 1 in Scheme 1). This phenomenon possibly leads to the following results: (1) compared to the non-compact powders (Conventional solid state route in Scheme 1), the reactants more easily contact with each other and conveniently diffuse in the pressed dense pellet. As a result, the BN crystallites grow larger, but the low temperature conditions prohibited the improvement of BN crystallinity. Thus poorly crystallized tBN micro-flakes are obtained (ESI S-2†); (2) gas products of the reaction, such as  $\text{NH}_3$ ,  $\text{N}_2$  and  $\text{H}_2$ , could not easily escape from the pressed dense pellet, and squash together to form high pressure tiny regions (see the bottom-left inset in Scheme 1). Within these regions, freshly formed tBN with poor crystallinity might partly convert to the cubic phase by the *in situ* phase transformation process (see Route 1 in Scheme 1). It is revealed that because cBN is the stable phase under high pressure, the close contact between reactants and the existence of high pressure tiny regions in the pressed dense pellets are beneficial to the formation of cBN by the *in situ* phase transformation process. If the stress inside the pellets can be so profitable, how about applying a constant pressure to the pellets,

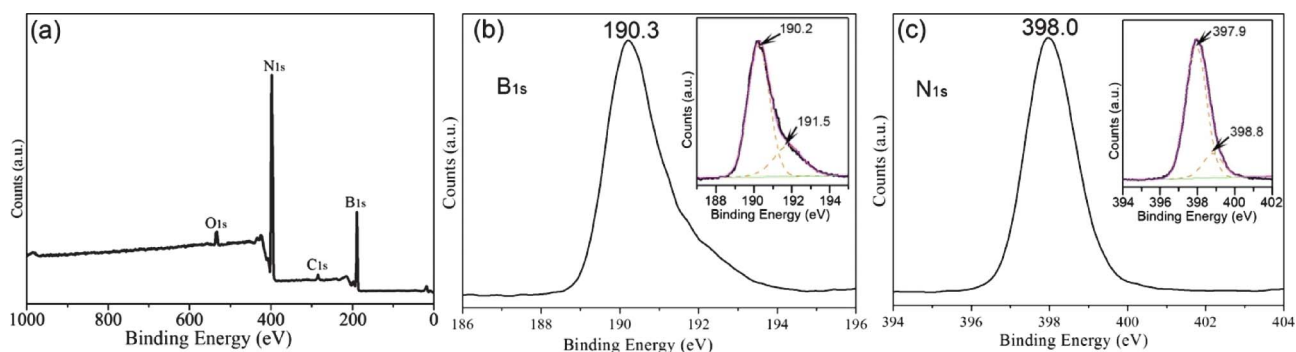


**Fig. 2** XPS spectra of sample S-1. (a) Survey spectrum; (b) spectrum of  $\text{B}_{1s}$ . Inset is the fitting result for the  $\text{B}_{1s}$  spectrum; (c) spectrum of  $\text{N}_{1s}$ . Inset is the fitting result for the  $\text{N}_{1s}$  spectrum.

as shown the Route 2 in Scheme 1? Otherwise, the escape of gas products from the pellets can be greatly suppressed by applying a direct pressure.

### 3.2 Formation of cBN *via* a solid state synthesis and *in situ* phase transformation with pressure assistance

In the following experiments,  $\text{NH}_4\text{BF}_4$  and  $\text{NaN}_3$  are selected as the reactants, and a series of BN samples are prepared *via* Route 2. The detailed experimental parameters are shown in Table 2. We mainly investigate the effects of temperature, pressure and duration for the phase transformation of turbostratic to cubic phase.

The as-obtained BN samples (S-6 to S-20) were characterized by FTIR spectra, as shown in Fig. 3. The peaks of  $1386\text{--}1415\text{ cm}^{-1}$  and  $772\text{--}805\text{ cm}^{-1}$  are attributed to  $\nu(\text{B-N})$  and  $\delta(\text{B-N})$  modes of tBN, respectively. The peaks of  $1050\text{--}1108\text{ cm}^{-1}$  come from the absorption of the TO phonon of cBN.<sup>31–32</sup> As is expected, the relative content of cBN rapidly increases with improving the pressure and prolonging the reaction duration at  $220\text{ }^\circ\text{C}$ , and finally, cBN becomes the dominant phase in sample S-10 prepared at  $450\text{ MPa}$  &  $220\text{ }^\circ\text{C}$  for  $48\text{ h}$ . With increasing the temperature to  $250\text{ }^\circ\text{C}$  and  $300\text{ }^\circ\text{C}$ , a similar phase transformation trend from tBN to cBN can be also observed. But because the freshly synthesized tBN at lower temperature presents poorer crystallinity, the *in situ* phase transformation extent of BN at  $220\text{ }^\circ\text{C}$  is obviously stronger than that of  $250\text{ }^\circ\text{C}$  and  $300\text{ }^\circ\text{C}$  at the same pressure.

In order to quantitatively analyze the variation of cBN concentrations in the as-prepared BN samples, we fitted the FTIR peaks by multi-Gaussian curves and evaluated the relative content of cBN *via* eqn (1):

$$\text{cBN}\% = \frac{I_{\text{cBN}}}{I_{\text{cBN}} + I_{\text{tBN}}} \times \% \quad (1)$$

wherein,  $I_{\text{cBN}}$  (at  $\sim 1079\text{ cm}^{-1}$ ) and  $I_{\text{tBN}}$  (at  $\sim 1400\text{ cm}^{-1}$ ) stand for the absorption peak areas of cBN and tBN, respectively. A diagram

depicting the relationship between cBN concentration and the pressure/temperature/duration is drawn in S-3 in the ESI.†

### 3.3 Fabrication of nearly pure cBN nanocrystals under the structural induction effect

Furthermore, for obtaining pure cBN by the low-temperature solid state synthesis and *in situ* phase transformation route, herein we introduce the structural induction effect. NaF displays an analogous face center cubic structure (fcc) to cBN and might induce the tBN transforming into cBN. All the other experimental parameters are the same as that of samples S-12 and S-14 (Table 2). In our experiments,  $5\text{ mmol}$  NaF were added into the reactants (Table 3), and the FTIR spectra of the BN samples are shown in Fig. 4. By comparing the spectra of samples S-12 and S-21, it is quite clear that the peak of cBN centered at  $1103\text{ cm}^{-1}$  is rather weak without the assistance of the structural induction effect, which indicates that only a small amount of cBN has formed on this occasion. But when NaF is introduced into the reactants, this peak of cBN centered at  $1098\text{ cm}^{-1}$  becomes the strongest peak and cBN is the dominant phase in this sample S-21. Furthermore, with increasing the pressure to  $450\text{ MPa}$ , the *in situ* phase transformation of tBN to cBN is performed more completely. By evaluating the cBN concentration of sample S-22 *via* eqn (1), an almost pure cBN ( $\sim 90\%$ ) sample is obtained.

**Table 3** Key parameters of preparing BN samples under the structural induction effect

No.	$\text{NH}_4\text{BF}_4/\text{NaN}_3/\text{NaF}$	$T\text{ (}^\circ\text{C)}$	$t\text{ (h)}$	$P\text{ (MPa)}$	Phases <sup>a</sup>
S-12	1/3/0	250	24	125	t*BN+cBN
S-21	1/3/0.5	250	24	125	tBN+cBN*
S-22	1/3/0.5	250	24	450	tBN+cBN*

<sup>a</sup> \* Denotes the dominant phase.

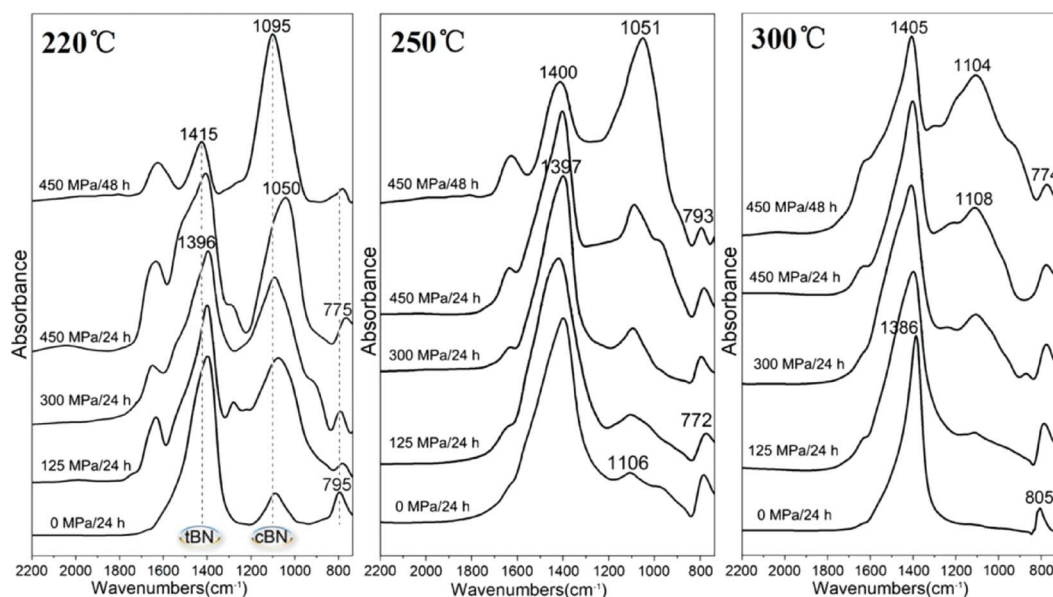


**Fig. 3** FTIR spectra of BN samples prepared by solid state synthesis and *in situ* phase transformation process under constant pressure. The peaks within  $1050\text{--}1108\text{ cm}^{-1}$  are attributed to the absorption of cBN, and those at  $1386\text{--}1415\text{ cm}^{-1}$  and  $772\text{--}805\text{ cm}^{-1}$  come from the absorption of tBN.

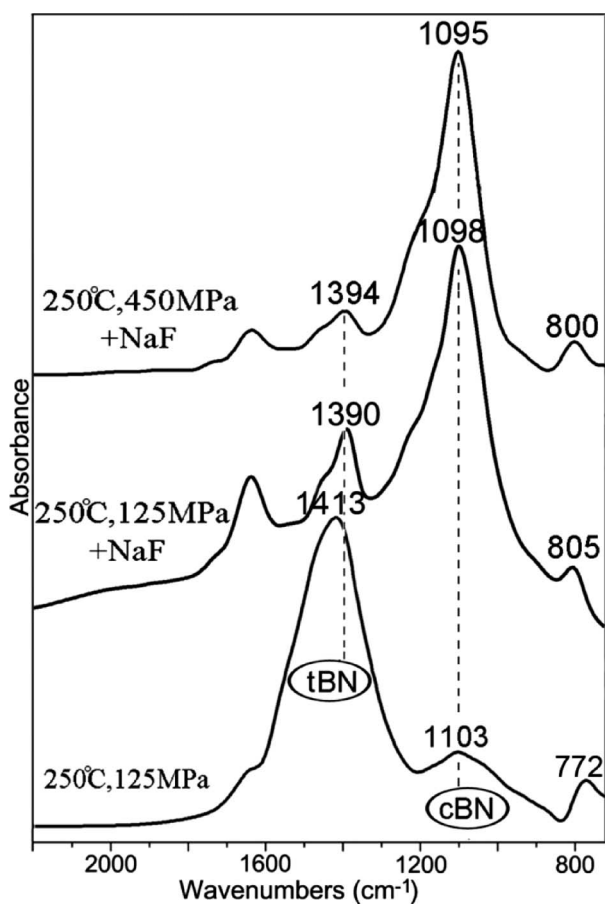


**Fig. 4** FTIR spectra of BN samples prepared under the structural induction effect. The peaks at 1390–1413  $\text{cm}^{-1}$  and 772–805  $\text{cm}^{-1}$  come from the absorption of tBN, while those at 1095–1103  $\text{cm}^{-1}$  should be attributed to the absorption of cBN. All the samples were prepared by reacting  $\text{NH}_4\text{BF}_4$  and  $\text{NaN}_3$  at 250 °C for 24 h. Besides, 5 mmol NaF was used as the structural induction material.

The XPS spectra were employed to determine the chemical bonding of samples S-12 and S-22, which are mainly composed of tBN and cBN, respectively. The peaks of  $\text{C}_{1s}$ ,  $\text{O}_{1s}$ ,  $\text{B}_{1s}$  and  $\text{N}_{1s}$  can be observed on the survey spectra shown in Fig. 5(a–b). The  $\text{C}_{1s}$  peak at 284.6 eV, which derives from surface contamination because the samples have been exposed to air before the XPS measurements, has been used to calibrate all the spectra due to the charging effect. The quantification of peaks shows that the atomic ratios of B : N are  $\sim 0.98 : 1$  for S-22 and  $\sim 1.05 : 1$  for S-12, respectively, which are very close to the chemical stoichiometry of BN. Besides, it is well known that XPS is an effective method to characterize cBN. It has been reported that only  $\text{sp}^2$ -bonded BN (tBN) shows a bump of  $\pi$  plasmon ( $\pi\text{P}$ ) loss peak at  $\sim 9$  eV away from the  $\text{B}_{1s}$  and  $\text{N}_{1s}$  spectra, but the peak does not appear in the  $\text{sp}^3$ -bonded cBN phase. This difference is usually used to distinguish  $\text{sp}^2$  and  $\text{sp}^3$  hybrid BN phases.<sup>34–36</sup> After carefully comparing Fig. 5(c) and (d), two  $\pi\text{P}$  loss peaks centered at  $\sim 9$  eV away from  $\text{B}_{1s}$  and  $\text{N}_{1s}$  peaks of sample S-12 are obviously found. However, no such  $\pi\text{P}$  peaks exist for sample S-22. Furthermore, the binding energies of the  $\text{B}_{1s}$  and  $\text{N}_{1s}$  peaks of sample S-12 and S-22 are characteristic of the tBN phase ( $190.0 \pm 0.1$  eV for  $\text{B}_{1s}$  and  $398.0 \pm 0.1$  eV for  $\text{N}_{1s}$ ) and cBN phase ( $191.0 \pm 0.1$  eV for  $\text{B}_{1s}$  and  $398.6 \pm 0.1$  eV for  $\text{N}_{1s}$ ),

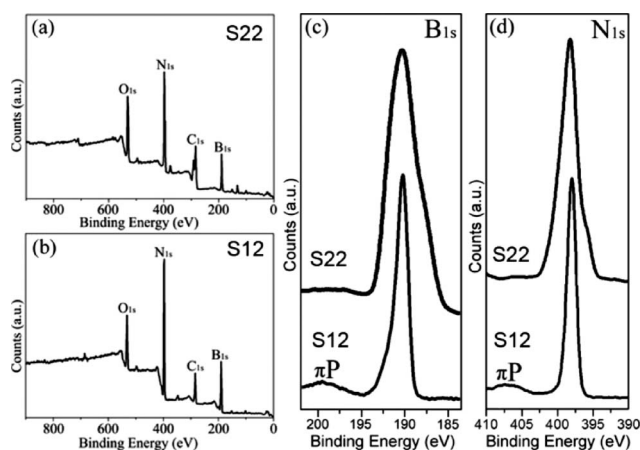


**Fig. 5** XPS spectra of samples S-12 and S-22. (a) Survey spectrum of sample S-22; (b) survey spectrum of sample S-12; (c)  $\text{B}_{1s}$  spectra of samples S-12 and S-22; (d)  $\text{N}_{1s}$  spectra of samples S-12 and S-22.  $\pi\text{P}$ :  $\pi$  plasmon.

respectively.<sup>34–38</sup> Therefore, both the  $\pi$  plasmon and the values of the binding energies support that sample S-22 is mainly composed of cBN, while the dominant phase of S-12 is tBN. The conclusion is also in good agreement with the FTIR results.

In addition, at another temperature and reactant system, the structure induction material also presents a positive influence for the *in situ* phase transformation of BN (ESI S-4†).

TEM was used to observe the micro-morphology of the almost pure cBN phase of sample S-22. Fig. 6(a) exhibits the typical images of cBN nanocrystals with diameters in the range of 30–60 nm. The corresponding SAED pattern taken from these nanocrystals reveals the cubic structure characteristic of the BN sample. The diffraction rings can be indexed to the (111), (200), (220) and (311) planes of cBN, respectively. In addition, the corresponding XRD pattern of sample S-22 is also presented in the ESI (Fig. S5)†

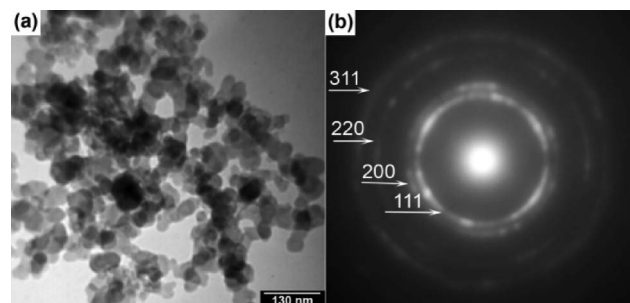


**Fig. 6** (a) TEM image of cBN nanocrystals; (b) the corresponding SAED pattern of cBN nanocrystals. The diffraction rings can be indexed to the (111), (200), (220) and (311) planes of cBN, respectively.

Besides, HRTEM was also used to identify the existence of cBN nanocrystals in sample S-22. Fig. 7(a) presents the residual tBN of sample S-22. The interlayer distance of (002) planes is  $\sim 3.5$  Å. Actually, the poor crystallinity can facilitate the *in situ* phase transformation of tBN to cBN. Fig. 7(b) displays the lattice fringes of cBN. The regular fringes reveals good crystallinity of cBN nanocrystals with a  $d$  value of 2.08 Å, which can be indexed to the (111) plane of cBN. Fig. 7(c) shows a typical cBN nanocrystal with  $\sim 60$  nm in

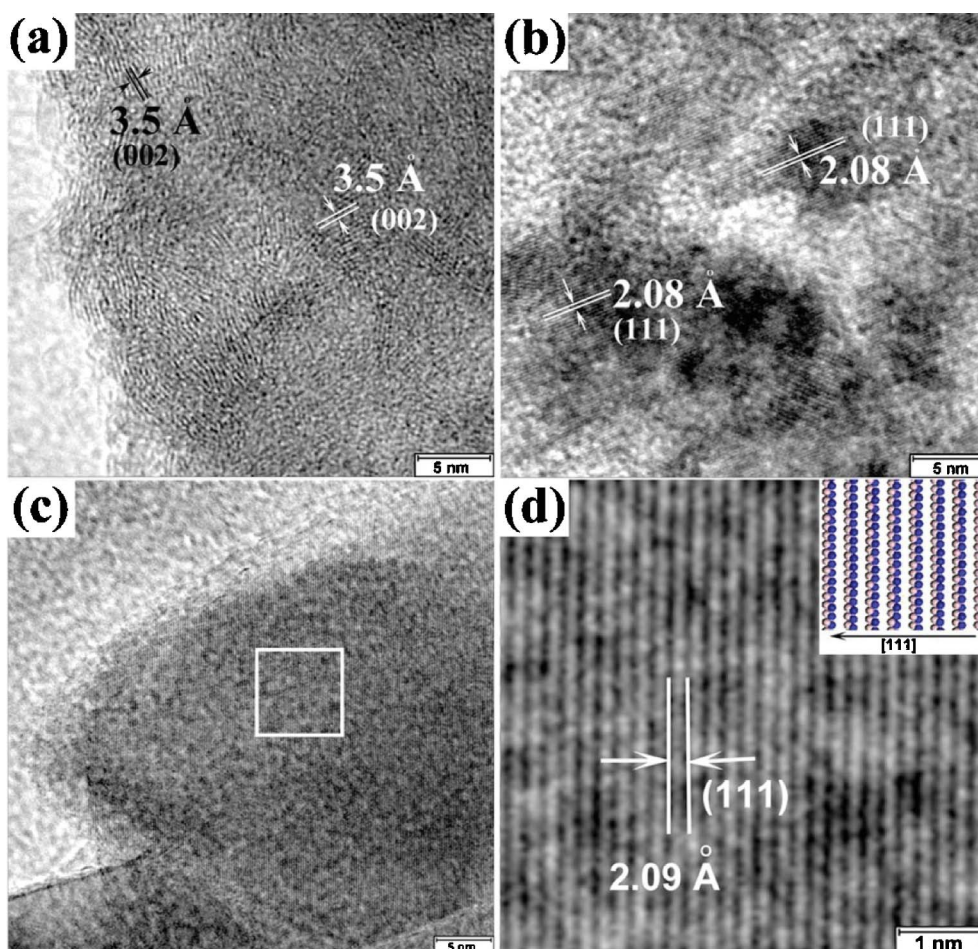


**Fig. 7** (a) HRTEM image of residual tBN in sample S-22; (b) HRTEM image of cBN nanocrystals in sample S-22; (c) a typical cBN nanocrystal; (d) high-magnification image of lattice fringes labeled by the box in (c). Inset is the corresponding structure model of cBN along the [111] direction.

size. The high-magnification of the HRTEM image presents well the single crystal properties of the cBN nanocrystal and obvious oriented growth of the {111} planes of cBN (Fig. 7(d)).

These above measurement results indicate that almost pure cBN phase can be fabricated *via* the low-temperature solid state synthesis and *in situ* phase transformation route with the help of the structural induction effect. This induction effect can be explained by the heterogeneous nucleation model, which deals with the nucleation barrier of a new born phase. If there are no foreign particles, cBN would nucleate spontaneously *via* phase transformation at the first step. It needs to overcome an energy barrier of  $\Delta G_{\text{hom}}$ . On the contrary, with the existence of foreign particles with fcc structure, cBN would prefer to nucleate on the surfaces of them, and the nucleation process becomes heterogeneous. In this case, the energy barrier reduces to  $\Delta G_{\text{het}}$  as follows:<sup>39</sup>

$$\Delta G_{\text{het}} = \Delta G_{\text{hom}} \left[ \frac{(2 + \cos \theta)(1 - \cos \theta)^2}{4} \right] \quad (2)$$

here  $\theta$  is the contact angle between the foreign particles and cBN, and is within the range of  $0 < \theta < 180^\circ$ .  $\Delta G_{\text{hom}}$  and  $\Delta G_{\text{het}}$  are the energy barriers of the homogeneous and heterogeneous

nucleation processes, respectively. Apparently,  $\Delta G_{\text{hom}} > \Delta G_{\text{het}}$ , and the smaller  $\theta$  is, the lower  $\Delta G_{\text{het}}$  is required. This fact indicates that a homogeneous nucleation process is more difficult than a heterogeneous one.

It is well known that cBN is a stable phase under high pressure, and it is difficult to synthesize cBN under ambient pressure. However, if foreign particles with fcc structure are introduced into the reaction system, the nucleation of cBN changes from homogeneous to heterogeneous, and the energy barrier decreases from  $\Delta G_{\text{hom}}$  to  $\Delta G_{\text{het}}$ . In other words, the formation of cBN crystallites becomes much easier on this occasion. As a result, the relative content of cBN obviously increases and an almost pure cubic phase BN sample is obtained when the structural induction material is added.

Except for the induction effect, NaF with fcc structure seems to play an important role in the oriented growth of {111} planes of cBN nanocrystals. In the NaF sponge, a lot of {111} planes are expected to be randomly exposed. So, while inducing the *in situ* phase transformation of tBN to cBN, the foreign NaF can be used as a template and promote the oriented growth of cBN nanocrystals on its surface. In contrary, when no foreign NaF is added in the reacting system, so obvious oriented characteristics of the cBN nanoparticles are not easily observed.

## 4. Conclusion

cBN is prepared by a low-temperature solid state synthesis and *in situ* phase transformation route, and the cBN concentration in the BN sample has been greatly increased by utilizing two new strategies, *i.e.*, applying pressure onto the reactants during the reaction process and introducing the structural induction effect. Finally, almost pure cBN sample is synthesized by reacting  $\text{NH}_4\text{BF}_4$  and  $\text{NaN}_3$  at 250 °C. In fact, the conventional solid state route is generally regarded as a facile and convenient route to synthesize hBN or tBN, and it is rather difficult to prepare cBN by this method. However, the modified solid state route reported in this paper has been proved to be very effective for increasing the relative content of cBN, but the actual yield of cBN is not high. It is reasonable to believe that, by applying these strategies and optimizing the preparation parameters, pure cBN will be synthesized with high yield soon.

## Acknowledgements

This work was supported financially by the Natural Science Foundation of China (50672048, 21073107, 50990061), the China Postdoctoral Science Foundation (20100481245), the Foundation of Shandong Science & Technology Council (2008GG30003008), Postdoctoral Innovation Foundation of Shandong Province (201003077), Independent Innovation Foundation of Shandong University (11250070611039) and Postdoctor Foundation of Shandong University (10000080962080).

## Notes and references

- P. B. Mirkarimi, K. F. McCarty and D. L. Medlin, *Mater. Sci. Eng., R*, 1997, **21**, 47.
- I. Tsiaoussis and N. Frangis, *J. Microsc.*, 2006, **223**, 205.
- J. Yu, Z. Zheng, H. C. Ong, K. Y. Wong, S. Matsumoto and W. M. Lau, *J. Phys. Chem. B*, 2006, **110**, 21073.
- O. Mishima, K. Era, J. Tanaka and S. Yamaoka, *Appl. Phys. Lett.*, 1988, **53**, 962.
- O. Mishima, J. Tanaka, S. Yamaoka and O. Fukunaga, *Science*, 1987, **238**, 181.
- E. Knittle, R. M. Wentzcovitch, R. Jeanloz and M. L. Cohen, *Nature*, 1989, **337**, 349.
- W. J. Zhang, X. M. Meng, C. Y. Chan, K. M. Chan, Y. Wu, I. Bello and S. T. Lee, *J. Phys. Chem. B*, 2005, **109**, 16005.
- J. B. MacNaughton, A. Moewes, R. G. Wilks, X. T. Zhou, T. K. Sham, T. Taniguchi, K. Watanabe, C. Y. Chan, W. J. Zhang, I. Bello, S. T. Lee and H. Hofsass, *Phys. Rev. B*, 2005, **72**, 195113.
- F. P. Bundy and R. H. Wentorf, *J. Chem. Phys.*, 1963, **38**, 1144.
- V. L. Solozhenko and V. Z. Turkevich, *J. Phys. Chem. B*, 1999, **103**, 8137.
- S. K. Singhal and J. K. Park, *J. Cryst. Growth*, 2004, **260**, 217.
- H. Lorenz and I. Orgzall, *Diamond Relat. Mater.*, 1995, **4**, 1046.
- V. Turkevich, T. Taniguchi, A. Andreev and P. Itsenko, *Diamond Relat. Mater.*, 2004, **13**, 64.
- J. Gijjna, H. J. Meurer, G. Nover, T. Peun, D. Schiinbohm and G. Will, *Mater. Lett.*, 1998, **33**, 321.
- X. C. Wang, X. P. Jia, T. C. Zhang, G. Z. Ren, H. J. Liu, C. Y. Zang, P. W. Zhu, H. A. Ma and G. T. Zou, *Diamond Relat. Mater.*, 2003, **12**, 57.
- M. M. Bindal, B. P. Singh, S. K. Singhal, R. K. Nayar and R. Chopra, *J. Cryst. Growth*, 1994, **144**, 97.
- J. Y. Huang and Y. T. Zhu, *Chem. Mater.*, 2002, **14**, 1873.
- V. L. Solozhenko, V. Z. Turkevich and G. Will, *High Press. Res.*, 1996, **10**, 135.
- E. G. Gillan and R. B. Kaner, *Chem. Mater.*, 1996, **8**, 333.
- L. Rao and R. B. Kaner, *Inorg. Chem.*, 1994, **33**, 3210.
- V. L. Solozhenko, V. Z. Turkevich and G. Will, *J. Am. Ceram. Soc.*, 1996, **79**, 2798.
- J. H. Ma, J. Li, G. X. Li, Y. G. Tian, J. Zhang, J. F. Wu, J. Y. Zheng, H. M. Zhuang and T. H. Pan, *Mater. Res. Bull.*, 2007, **42**, 982.
- C. H. Wallace, S. H. Kim, G. A. Rose, L. Rao, J. R. Heath, M. Nicol and R. B. Kaner, *Appl. Phys. Lett.*, 1998, **72**, 596.
- J. L. O'Loughlin, C. H. Wallace, M. S. Knox and R. B. Kaner, *Inorg. Chem.*, 2001, **40**, 2240.
- A. Spiesser, Y. M. Chong, K. M. Leung, G. Abel, G. G. Ross, M. J. Walzak, R. Jachlin, W. M. Lau, W. J. Zhang and I. Bello, *J. Phys. Chem. C*, 2007, **111**, 12768.
- X. W. Zhang, H. G. Boyen, N. Deyneka, P. Ziemann, F. Banhart and M. Schreck, *Nat. Mater.*, 2003, **2**, 312.
- W. J. Zhang, I. Bello, Y. Lifshitz, K. M. Chan, X. M. Meng, Y. Wu, C. Y. Chan and S. T. Lee, *Adv. Mater.*, 2004, **16**, 1405.
- D. D. Nataliya, U. Herr, H. J. Fecht, X. W. Zhang, H. Yin, H. G. Boyen and P. Ziemann, *Adv. Eng. Mater.*, 2008, **10**, 482.
- J. F. Moulder, W. F. Stickle, P. E. Sobol and K. D. Bembem, *Handbook of X-ray Photoelectron Spectroscopy, Physical Electronics, Division*, Perkin-Elmer Corporation, 1992.
- C. C. Tang, Y. Bando, Y. Huang, C. Y. Zhi and D. Golberg, *Adv. Funct. Mater.*, 2008, **18**, 3653.
- K. M. Leung, C. Y. Chan, Y. M. Chong, Y. Yao, K. L. Ma, I. Bello, W. J. Zhang and S. T. Lee, *J. Phys. Chem. B*, 2005, **109**, 16272.
- U. Vetter, P. Reinke, C. Ronning, H. Hofsass, P. Schaaf, K. Bharuth-Ram and T. Taniguchi, *Diamond Relat. Mater.*, 2003, **12**, 1182.
- B. E. Douglas, D. H. McDaniel and J. J. Alexander, *Concepts and Model of Inorganic Chemistry*, 2nd Edition, Wiley, New York 1983.
- K. S. Park, D. Y. Lee, K. J. Kim and D. W. Moon, *Appl. Phys. Lett.*, 1997, **70**, 315.
- L. D. Jiang, A. G. Fitzgerald, M. J. Rose, A. Lousa and S. Gimeno, *Surf. Interface Anal.*, 2002, **34**, 732.
- B. Angleraud, M. Cahoreau, I. Jauberteau, J. Aubreton and A. Catherinot, *J. Appl. Phys.*, 1998, **83**, 3398.
- K. Nose, H. S. Yang, H. Oba and T. Yoshida, *Diamond Relat. Mater.*, 2005, **14**, 1960.
- J. B. Lian, T. Kim, X. D. Liu, J. M. Ma and W. J. Zheng, *J. Phys. Chem. C*, 2009, **113**, 9135.
- C. H. L. Goodman, *Crystal Growth Theory and Techniques*, Plenum Press-London-New York, 1974, Chapter 2.